Molecular signature and functional properties of human pluripotent stem cell-derived brain pericytes

Allison Bosworth*[1,2], Casey Griffin*[3,4], Ararat Chakhoyan*[1,2], Abhay P. Sagare*[1,2], Amy R. Nelson[1,2,5], Yaoming Wang[1,2], Kassandra Kisler[1,2], Axel Montagne[1,2,6], Veronica Clementel[1,2,7], Julia TCW [8], Ruslan Rust[1,2,9], Marcelo Coba**[1,2,7], Berislav V. Zlokovic**[1,2]

1 Department of Physiology and Neuroscience, University of Southern California, Los Angeles, CA 90089

2 Zilkha Neurogenetic Institute, Keck School of Medicine, University of Southern California, 1501 San Pablo St., Los Angeles, CA 90089

3 Eli and Edythe Broad Center for Regenerative Medicine, Department of Stem Cell Biology and Regenerative Medicine, Keck School of Medicine, University of Southern California, Los Angeles, CA 90089

4 Department of Molecular Pathobiology, New York University, New York, United States

5 Department of Physiology and Cell Biology, University of South Alabama, Mobile, AL

6 UK Dementia Research Institute at the University of Edinburgh, Centre for Clinical Brain Sciences, Chancellor's Building, Edinburgh Medical School, EH16 4SB, UK.

7 Department of Psychiatry and Behavioral Sciences, Keck School of Medicine, University of Southern California, Los Angeles, CA 90089

8 Department of Pharmacology, Physiology & Biophysics, Chobanian & Avedisian School of Medicine, Boston University, 700 Albany St., Boston, MA 02118

9 Institute for Regenerative Medicine (IREM), University of Zurich, Campus Schlieren, Wagistrasse 12, 8952, Schlieren, Switzerland

*co-first authors
**co-senior authors

Correspondence:

Berislav V. Zlokovic, M.D., Ph.D.
Email: zlokovic@usc.edu

Abstract

Brain pericytes maintain blood-brain barrier (BBB), secrete neurotrophic factors and clear toxic proteins. Their loss in neurological disorders leads to BBB breakdown, neuronal dysfunction, and cognitive decline. Therefore, cell therapy to replace lost pericytes holds potential to restore impaired cerebrovascular and brain functions. Here, we show by a quantitative analysis of 8,344 proteins and 20,572 phosphopeptides that human iPSC-derived brain pericytes (iPSC-PC) share 96% of total proteins and 98% of protein phosphorylation sites with primary human brain pericytes. This includes cell adhesion and tight junction proteins, transcription factors, and different protein kinase families of the human kinome. In pericyte-deficient mice, iPSC-PC home to host brain capillaries to form hybrid human-mouse microvessels. They repair BBB leaks and protect against neuron loss, which we show requires PDGRFB and pleiotrophin. They also clear Alzheimer's amyloid-β and tau neurotoxins via lipoprotein receptor. Thus, iPSC-PC may offer a valuable replacement therapy for pericyte-deficient neurological disorders.

Introduction

Pericytes are mural cells on brain capillaries that maintain blood-brain barrier (BBB) integrity and function [1–5]. They contribute to formation of new blood vessels [6], secrete neurotrophic factors [4], and clear toxic proteins such as Alzheimer's disease (AD) amyloid-β (Aβ) [7,8] and tau [9]. Their loss in neurodegenerative disorders such as AD and related disorders leads to BBB breakdown [6], is associated with synaptic and neuronal dysfunction [3,4,10] and can predict cognitive decline in individuals carrying the *ε4* variant of apolipoprotein E (*APOE4*), the main susceptibility gene for AD [11]. Therefore, replacing lost pericytes by induced pluripotent stem cell (iPSC)-derived therapies holds potential to restore impaired cerebrovascular and brain functions.

Different protocols have been developed to generate human iPSC-derived brain pericytes (iPSC-PC) [12–15]. iPSC-PC have been shown to enhance BBB integrity in human *in vitro* BBB models [12,13] and in a mouse model of ischemic stroke [14]. Additionally, it has been shown that iPSC-PC from *ε4/ε4* donors compared to *ε3/ε3* donors lead to a greater Aβ deposition in human BBB models [15] and activation of BBB-degrading cyclophilin A-matrix metalloproteinase-9 pathway [11].

Despite these advances, the molecular profile and functional properties of iPSC-PC are still poorly understood. Whether their molecular signaling machinery corresponds to primary adult human brain microvascular pericytes (PC) remains elusive. It is also unknown if the principal functional components of iPSC-PC including cell adhesion molecules, tight junction proteins, transcription factors, and the protein kinase families of the human kinome can recapitulate the signaling signatures and functions observed in PC. Moreover, in terms of function, whether iPSC-PC can home to brain capillaries that lost some of their own pericyte coverage to form new hybrid microvessels with the host vessels, whether they can repair BBB leaks, and whether they can protect against neuronal dysfunction associated with pericyte deficiency, remains elusive, and the underlying molecular mechanisms remain unstudied.

To address these questions, we performed a quantitative comparative analysis of total proteome and phosphoproteome of iPSC-PC and PC using liquid chromatography mass spectrometry (LC/MS). Next, we studied vasculogenic potential of iPSC-PC to form hybrid microvessels with the host brain capillaries in the hippocampus of pericyte-deficient mice, determined BBB integrity of newly-formed hybrid vessels, studied their effects on neuronal function, and evaluated their capability to remove Alzheimer's Aβ and tau neurotoxins.

Results

During *in vivo* development, CNS pericytes originate from either neuroectoderm or mesoderm. Neuroectoderm-derived neural crest cells (NCC) differentiate into pericytes of the forebrain while pericytes of the midbrain, brain stem, and spinal cord have mesodermal origin [16]. Therefore, to generate human forebrain pericytes (iPSC-PC) from iPSC, we used a modified two-step approach with a NCC intermediate similar to previous reports [12–14] (**Fig. 1a**).

Immunostaining revealed that iPSC-derived NCC express NCC markers p75 and SOX10, but have barely detectable or undetectable levels of pericyte markers PDGFRB and NG2 (**Supp. Fig. 1a-c**). After differentiation into iPSC-PC, a robust expression of PDGFRB and NG2 was observed (**Supp. Fig. 1b-c**). Immunoblotting confirmed that iPSC-PC and PC express high levels of several canonical pericyte markers including NG2 (CSPG4), PDGFRβ (PDGFRB), CD13 (ANPEP), Caldesmon (CALD1), and Vitronectin (VTN) (**Supp. Fig. 1d**). As anticipated, markers of endothelial cells (GLUT1, CD31), neurons (NFL, TUJ1), oligodendrocytes (CNPase, OLIG2), astrocytes (ALDH1, GFAP, S100B), microglia (CD11B, CD68, IBA1), and vascular smooth muscle cells (MYH11, ACTA2, CNN1) were not expressed in iPSC-PC or PC (**Supp. Fig. 2a-f**).

LC/MS analysis performed as we previously reported [10,17–20] allowed us to identify and quantitate 8,344 proteins and 20,572 phosphopeptides showing no significant changes between iPSC-PC and PC (q>0.01) in 8,027 proteins (96%) and 20,135 phosphopeptides (98%) (**Fig. 1b-d**). All proteomic and phosphoproteomic data are accessible via ProteomeXchange data base. Heatmap analysis of the top 50 most variably expressed proteins revealed a homogenous protein expression between iPSC-PC and PC, lacking any distinct pattern segregating the two groups (**Fig. 1c**). Volcano plot of common (8,027) and differentially expressed upregulated (134) or downregulated (183) proteins between iPSC-PC vs PC is shown in **Fig. 1d**.

LC/MS quantitative analysis of canonical pericyte markers including PDGFRβ (PDGFRB), Caldesmon (CALD1), NG2 (CSPG4), CD13 (ANPEP), and Vitronectin (VTN) indicated no changes in total protein levels or within 22 protein phosphopeptides between iPSC-PC and PC (**Fig. 1e**). Importantly, we did not observe changes in phosphorylation in regulatory sites on PDGFRB S712 and S1104, which are essential for PDGFRB activity and association in protein interaction networks.

We then asked if the same pattern is observed in the main functional components of iPSC-PC. Therefore, we analyzed changes in the total protein and protein phosphorylation in cell adhesion and tight junction proteins, transcription factors, and protein kinases. We observed no changes in total protein and phosphorylation levels within 17 cell adhesion proteins and 18 phosphopeptides (**Fig. 1f**). The same pattern was observed for tight junction proteins with no changes in protein levels in all studied proteins and all 114 phosphopeptides detected (**Fig. 1g),** including major components of the pericyte tight junctions such as TJP2, TJP3, GJA1, DLG1 and others. These results suggest that cell adhesion and tight junction functions are highly preserved in iPSC-PC.

To determine if the intracellular signaling machinery and output response of iPSC-PC resemble that of PC, we analyzed total protein and phosphorylation changes in the transcription factors and protein kinases detected. We observed no significant changes (q>0.01) in total protein content in 96% of 183 total transcription factors, nor in protein phosphorylation in 96% of 212 identified phosphopeptides within 52 transcription factors (**Fig. 2a**), suggesting no changes in the output response regulating total protein content in iPSC-PC. The analysis of the pericyte kinome allowed us to identify and quantitate a total of 275 protein kinases among all branches of the human kinome, including TK: Tyrosine kinase group; TKL: Tyrosine kinase-like group; STE: Sterile (homologs of yeast Ste7) group; CK1: Casein Kinase 1 group; AGC: Protein kinase A, Protein kinase B, Protein kinase C group; CAMK: Calmodulin calcium kinase group; CMGC [cyclin-dependent kinases (CDKs), mitogen-activated protein kinases (MAPKs), glycogen synthesis kinases (GSKs), and CDK-like kinases] group. We observed no significant changes

(q>0.01) in 94% of protein kinases (**Fig. 2b-c**). We also identified and quantitated 812 phosphopeptides with 636 unique phosphorylation sites within 160 protein kinases distributed among different families of the human kinome (**Fig. 2b,d**) with no significant changes (q>0.01) in 98% of phosphopeptides.

The activity of protein kinases is usually modulated by protein phosphorylation of key phosphorylation sites that regulate their intrinsic kinase activity, protein localization and association to protein partners [21]. Therefore, we identified protein kinase regulatory sites within the protein phosphorylation sites quantitated using the PhoshoSitePlus database resource followed by manual curation [22]. We were able to identify 117 regulatory phosphorylation sites distributed along different protein kinase families in the pericyte kinome. Protein quantitation showed no significant differences (q>0.01) in any of the identified regulatory phosphorylation sites (**Fig. 2d**). Altogether, these findings provide strong support for the high degree of similarity in the molecular signatures and functional capacity of iPSC-PC and PC, and suggest that iPSC-PC not only express similar protein levels in the main functional components of their total proteome as PC, but their protein functional characteristics are also preserved as we did not observe major changes in their phosphorylation signatures.

We next performed *in vitro* and *in vivo* experiments with iPSC-PC to evaluate their physiological functions. Since brain pericytes are known to enhance tight junction (TJ) formation between brain endothelial cells [2,3], we cultured mouse brain endothelial cell (EC) monolayers with iPSC-PC conditioned medium, and studied expression of TJ protein claudin-5. Consistent with previous reports showing that iPSC-PC can enhance integrity of endothelial monolayers in human *in vitro* BBB models [12,13], claudin-5 was expressed at significantly ($p < 0.05$) higher levels in EC monolayers exposed to iPSC-PC conditioned medium compared to EC medium only (**Supp. Fig. 3a-b**).

Then we asked whether iPSC-PC can home to brain capillaries in host brains that lost some of their own pericyte coverage. To address this question we studied integration of GFP-labeled iPSC-PC with brain capillaries of 6-8-month old pericyte-deficient *Pdgfrb*$^{F7/F7}$ (F7/F7) mice that exhibit approximately 40% loss of pericyte coverage [3,23]. First, we used an *in vitro* live brain slice model (**Fig. 3a**) in which iPSC-PC were seeded onto the top of brain slices and allowed to integrate with the tissue over 24 h. Since pericyte-endothelial PDGFRB/PDGFB signaling is a key mechanism by which pericytes are recruited to the vessel wall [24], we also studied whether silencing PDGFRB in iPSC-PC compared to si.*Control* (**Fig. 3b**) will have an effect on their integration with F7/F7 brain capillaries. This experiment revealed that within 24 h after adding iPSC-PC to brain slices > 80% of GFP-iPSC-PC transduced with si.*Control* homed to the host brain capillaries to form hybrid vessels, and exhibited elongated cellular morphologies similar to native, endogenous pericytes (**Fig. 3c**). However, after PDGFRB silencing (**Fig. 3c**), iPSC-PC no longer homed to capillaries (**Fig. 3c, d**).

To assess if the homing effect can be also seen *in vivo,* we next transplanted GFP-iPSC-PC into the hippocampi of F7/F7 mice (**Fig. 3e**). Similar to the *ex vivo* results, iPSC-PC transduced with si.*Control* homed to brain capillaries of F7/F7 mice *in vivo* within 24 h of grafting, while the effect was lost after PDGFRB silencing (**Fig. 3f**). Within 5 days of grafting, > 40% of transplanted GFP-iPSC-PC transduced with si.*Control* were associated with brain capillaries of F7/F7 mice, which again was abolished by PDGFRB silencing (**Fig. 3f-h**). Altogether, these data show that iPSC-PC home to and enwrap pericyte-deficient brain capillaries to form a hybrid human-mouse microvascular formations, which required PDGFRB.

We next sought to determine if transplanted iPSC-PC can restore functionally the BBB integrity in hippocampi of 6-8-month old F7/F7 mice, which exhibit substantial BBB leakage consequent to pericyte loss [3,4]. Using dynamic contrast-enhanced magnetic resonance imaging (DCE-MRI) [4,25] we quantified the unidirectional BBB permeability constant K_{trans} in the hippocampus, a site of the iPSC-PC injections, and the striatum, a region distant of the site of iPSC-PC injections. (**Fig. 4a**). This experiment confirmed that control F7/F7 mice treated with

vehicle have 65-70% higher K_{trans} BBB permeability values compared to age-matched controls on the same genetic background, indicating a leakier BBB as reported [3,4] (**Fig. 4b,c**). However, F7/F7 mice transplanted with iPSC-PC transduced with si.*Control* showed substantially improved BBB permeability in the hippocampus, similar to values found in normal control mice on the same genetic background (**Fig. 4b,c**). The restoration of BBB integrity was seen in the hippocampus, a site of iPSC-PC grafting, but did not extend to regions distant from the grafting site such as striatum (**Fig. 4 b,d**). PDGFRB silencing abolished protective effects of iPSC-PC on BBB integrity, and the K_{trans} values remained similar as found in untreated F7/F7 mice.

To determine whether grafting of iPSC-PC can influence neurodegenerative process in F7/F7 mice we stained hippocampal tissue with NeuN and SMI312 and determined neuronal counts and neuritic density, respectively, as previously reported [4,25] (**Fig. 4e-g**). Consistent with previous reports, 6-8-month old F7/F7 mice displayed 30% lower neuronal counts and 20% lower neuritic density compared to age-matched control mice on the same genetic background [3] (**Fig. 4f,g**). Treatment of F7/F7 mice with iPSC-PC transduced with si.*Control* had a substantial neuroprotective effect, as shown by 77% increase in NeuN-positive cells and 80% increase in SMI312 neuritic density in the CA1 region of the hippocampus, which was abolished by PDGFRB silencing (**Fig. 4e-g**). This data suggests that iPSC-PC therapy not only restores BBB integrity but also provides neuroprotection.

Since pleiotrophin (PTN), a neurotrophic factor secreted by brain pericytes, supports neuronal survival [4,26], we next studied whether silencing PTN has an effect on neuroprotective activity of iPSC-PC. First, we found that PTN silencing did not result in loss of vasculoprotective effect of iPSC-PC in F7/F7 mice (**Fig. 4b-c**) consistent with a previous report showing that intracerebroventricular infusion of PTN does not affect vasculature in mice with inducible pericyte loss [4]. However, grafting of iPSC-PC transduced with si.*PTN* compared to si.*Control* in F7/F7 mice diminished by 46% ($p < 0.05$) and 32% ($p < 0.001$) the number of NeuN-positive neurons and SMI312-positive neuritic density, respectively (**Fig. 4f-g**), suggesting that iPSC-PC can promote neuronal survival not only by restoring the BBB integrity, but also by direct neuroprotection via PTN.

Since mouse pericytes have been shown to clear Aβ [7,8] and tau [9] from brain, we also studied whether our iPSC-PC are capable of clearing Aβ and tau. First, iPSC-PC were seeded onto coverslips coated with Cy3-labeled Aβ42, as we reported [27,28]. After 5 days of incubation with iPSC-PC, we found approximately 80% reduction in coverslip-bound Cy3-Aβ42 compared to coverslips without cells (**Fig. 5a**). When LRP1, a major Aβ clearance receptor [29,30], was silenced in iPSC-PC, no Aβ clearance was observed (**Fig. 5a**). iPSC-PC were also seeded onto blank coverslips and incubated with soluble Cy3-labeled tau. After 48 hours, Cy3-tau was internalized and degraded by iPSC-PC (**Fig. 5b**). Silencing LRP1, which acts as a master regulator of tau uptake [31], significantly reduced Cy3-tau uptake in iPSC-PC by 74% (**Fig. 5b, c**). Together, these data suggest that iPSC-PC clear both Aβ and tau via an LRP1-dependent mechanism similar to mouse pericytes.

Discussion

Earlier characterization of iPSC-PC and primary brain PC relied on a relatively limited set of 4-10 pericyte markers and/or proteins known to be expressed by pericytes [12–14]. While one study suggested parallels between iPSC-PC and brain PC using bulk RNAseq, the work focused on transcript presence or absence, leaving the statistical analysis of differential gene expression unexplored [13]. Moreover, these previous studies [12–14] compared iPSC-PC to commercial human 'primary brain pericytes' of unspecified origin, likely derived from human fetal tissue. A fetal pericyte origin is also suggestive from the high expression of ACTA2, which has not been observed in iPSC-PC and PC in the present study, or in pericytes from two recent single-cell

atlases of the human adult brain vasculature [32,33], but rather is found in immature pericytes [34]. In contrast, here we performed the first comprehensive analysis of global protein expression in iPSC-PC and PC, which revealed highly shared proteome with preserved functional characteristics of proteins as indicated by their comparable phosphorylation signatures, and with preserved multiple physiological functions of pericytes as shown by different experimental models.

Using a quantitative LC/MS comparative analysis of 8,344 proteins and 20,572 phosphopeptides, we showed that human iPSC-PC share 96% of total proteins and 98% of protein phosphopeptides with primary human brain PC including canonical pericyte markers, cell adhesion and tight junction proteins, transcription factors, and the protein kinase families of the human kinome.

We then showed that iPSC-PC home to brain capillaries of pericyte-deficient F7/F7 mice on *ex vivo* brain slices, and *in vivo* after grafting into the hippocampus suggesting their vasculogenic potential to form hybrid vessels with the host vessels, which we show requires PDGFRB. Using our DCE-MRI technique [4,25] we showed that iPSC-PC grafting into the hippocampus restores BBB permeability to control mouse levels in F7/F7 mice. Moreover, transplantation of iPSC-PC into the F7/F7 mouse hippocampus increased neuronal counts and neuritic density. Importantly, this neuroprotective effect of iPSC-PC required both PDGFRB and the neurotrophic factor PTN. Finally, we showed that iPSC-PC clear Alzheimer's Aβ and tau proteins via LRP1, similar as previously shown in mice [29,30,31].

In conclusion, the present study provides support for potentially translating iPSC-PC for use in humans to restore impaired cerebrovascular and brain functions. In this regard, the autologous patient-derived iPSC-PC brain transplants may hold potential as a valuable cell replacement therapy for neurological disorders associated with pericyte deficiency such as for example AD and related disorders [6] characterized with cerebrovascular changes and BBB breakdown, loss of neurons and impaired clearance of Alzheimer's Aβ and tau neurotoxins.

1. Armulik, A. *et al.* Pericytes regulate the blood–brain barrier. *Nature* **468**, 557–561 (2010).
2. Daneman, R., Zhou, L., Kebede, A. A. & Barres, B. A. Pericytes are required for blood–brain barrier integrity during embryogenesis. *Nature* **468**, 562–566 (2010).
3. Bell, R. D. *et al.* Pericytes Control Key Neurovascular Functions and Neuronal Phenotype in the Adult Brain and during Brain Aging. *Neuron* **68**, 409–427 (2010).
4. Nikolakopoulou, A. M. *et al.* Pericyte loss leads to circulatory failure and pleiotrophin depletion causing neuron loss. *Nat Neurosci* **22**, 1089–1098 (2019).
5. Ayloo, S. *et al.* Pericyte-to-endothelial cell signaling via vitronectin-integrin regulates blood-CNS barrier. *Neuron* **110**, 1641-1655.e6 (2022).
6. Sweeney, M. D., Zhao, Z., Montagne, A., Nelson, A. R. & Zlokovic, B. V. Blood-Brain Barrier: From Physiology to Disease and Back. *Physiological Reviews* **99**, 21–78 (2019).
7. Sagare, A. P. *et al.* Pericyte loss influences Alzheimer-like neurodegeneration in mice. *Nat Commun* **4**, 2932 (2013).
8. Tachibana, M., Yamazaki, Y., Liu, C.-C., Bu, G. & Kanekiyo, T. Pericyte implantation in the brain enhances cerebral blood flow and reduces amyloid-β pathology in amyloid model mice. *Experimental Neurology* **300**, 13–21 (2018).
9. Ojo, J. *et al.* Mural cell dysfunction leads to altered cerebrovascular tau uptake following repetitive head trauma. *Neurobiology of Disease* **150**, 105237 (2021).
10. Barisano, G. *et al.* A “multi-omics” analysis of blood–brain barrier and synaptic dysfunction in APOE4 mice. *Journal of Experimental Medicine* **219**, e20221137 (2022).
11. Montagne, A. *et al.* APOE4 leads to blood–brain barrier dysfunction predicting cognitive decline. *Nature* **581**, 71–76 (2020).

12. Faal, T. *et al.* Induction of Mesoderm and Neural Crest-Derived Pericytes from Human Pluripotent Stem Cells to Study Blood-Brain Barrier Interactions. *Stem Cell Reports* **12**, 451–460 (2019).
13. Stebbins, M. J. *et al.* Human pluripotent stem cell–derived brain pericyte–like cells induce blood-brain barrier properties. *Science Advances* **5**, eaau7375 (2019).
14. Sun, J. *et al.* Transplantation of hPSC-derived pericyte-like cells promotes functional recovery in ischemic stroke mice. *Nat Commun* **11**, 5196 (2020).
15. Blanchard, J. W. *et al.* Reconstruction of the human blood–brain barrier in vitro reveals a pathogenic mechanism of APOE4 in pericytes. *Nat Med* **26**, 952–963 (2020).
16. Winkler, E. A., Bell, R. D. & Zlokovic, B. V. Central nervous system pericytes in health and disease. *Nat Neurosci* **14**, 1398–1405 (2011).
17. Li, J. *et al.* Long-term potentiation modulates synaptic phosphorylation networks and reshapes the structure of the postsynaptic interactome. *Science Signaling* **9**, rs8–rs8 (2016).
18. Li, J. *et al.* Spatiotemporal profile of postsynaptic interactomes integrates components of complex brain disorders. *Nat Neurosci* **20**, 1150–1161 (2017).
19. Wilkinson, B., Li, J. & Coba, M. P. Synaptic GAP and GEF Complexes Cluster Proteins Essential for GTP Signaling. *Sci Rep* **7**, 5272 (2017).
20. Wilkinson, B. *et al.* Endogenous Cell Type–Specific Disrupted in Schizophrenia 1 Interactomes Reveal Protein Networks Associated With Neurodevelopmental Disorders. *Biological Psychiatry* **85**, 305–316 (2019).
21. Kanev, G. K. *et al.* The Landscape of Atypical and Eukaryotic Protein Kinases. *Trends in Pharmacological Sciences* **40**, 818–832 (2019).

22. Hornbeck, P. V. *et al.* PhosphoSitePlus: a comprehensive resource for investigating the structure and function of experimentally determined post-translational modifications in man and mouse. *Nucleic Acids Res* **40**, D261–D270 (2012).
23. Nikolakopoulou, A. M., Zhao, Z., Montagne, A. & Zlokovic, B. V. Regional early and progressive loss of brain pericytes but not vascular smooth muscle cells in adult mice with disrupted platelet-derived growth factor receptor-β signaling. *PLOS ONE* **12**, e0176225 (2017).
24. Armulik, A., Genové, G. & Betsholtz, C. Pericytes: Developmental, Physiological, and Pathological Perspectives, Problems, and Promises. *Developmental Cell* **21**, 193–215 (2011).
25. Montagne, A. *et al.* Pericyte degeneration causes white matter dysfunction in the mouse central nervous system. *Nature Medicine* **24**, 326–337 (2018).
26. Vanlandewijck, M. *et al.* A molecular atlas of cell types and zonation in the brain vasculature. *Nature* **554**, 475–480 (2018).
27. Bell, R. D. *et al.* SRF and myocardin regulate LRP-mediated amyloid-beta clearance in brain vascular cells. *Nat Cell Biol* **11**, 143–153 (2009).
28. Ma, Q. *et al.* Blood-brain barrier-associated pericytes internalize and clear aggregated amyloid-β42 by LRP1-dependent apolipoprotein E isoform-specific mechanism. *Mol Neurodegener* **13**, 57 (2018).
29. Deane, R. *et al.* LRP/amyloid beta-peptide interaction mediates differential brain efflux of Abeta isoforms. *Neuron* **43**, 333–344 (2004).
30. Zhao, Z. *et al.* Central role for PICALM in amyloid-β blood-brain barrier transcytosis and clearance. *Nat Neurosci* **18**, 978–987 (2015).

31. Rauch, J. N. *et al.* LRP1 is a master regulator of tau uptake and spread. *Nature* **580**, 381–385 (2020).

32. Winkler, E. A. *et al.* A single-cell atlas of the normal and malformed human brain vasculature. *Science* **375**, eabi7377 (2022).

33. Yang, A. C. *et al.* A human brain vascular atlas reveals diverse mediators of Alzheimer's risk. *Nature* **603**, 885–892 (2022).

34. Guo, M. *et al.* Single cell RNA analysis identifies cellular heterogeneity and adaptive responses of the lung at birth. *Nat Commun* **10**, 37 (2019).

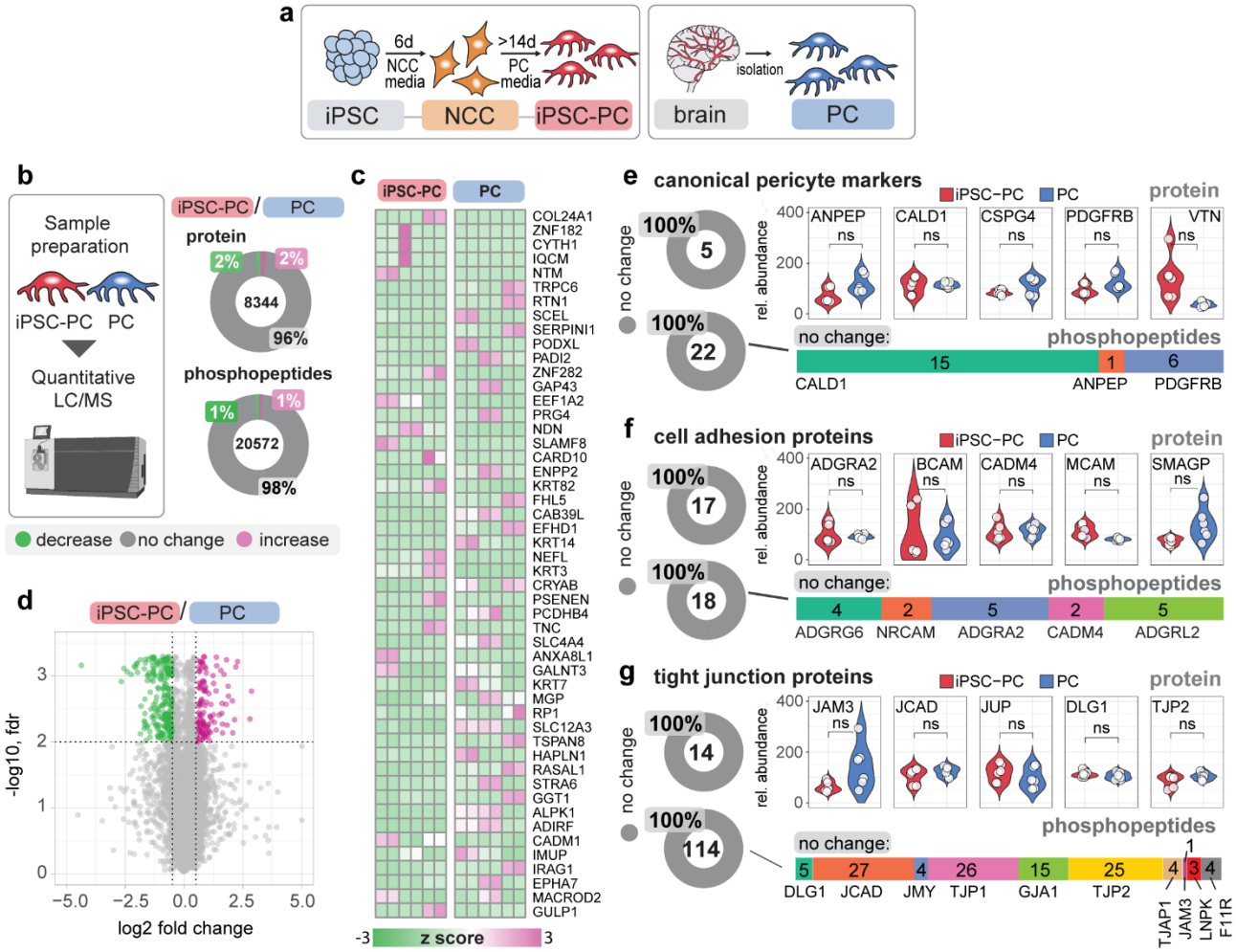

Figure 1. Generation and molecular characterization of iPSC-PC. (**a**) Schematic illustrating iPSC-PC were generated via a neural crest cell (NCC) intermediate, and primary human brain pericytes (PC) were isolated from postmortem cortical tissue. (**b**) Left: schematic illustrating proteomic data generation workflow by Liquid Chromatography/Mass Spectrometry (LC/MS). Right: Quantitative total proteome (top) and phosphoproteome (bottom) analysis of iPSC-PC vs. PC shown as donut plots (values inside plots represent total proteins/phosphopeptides; percentage indicates unchanged (grey), downregulated (green) and upregulated (magenta) proteins/phosphopeptides). (**c**) Heatmap of top 50 highly variant proteins between six independent cultures of iPSC-PC and PC. Protein expression is shown as a z score. Magenta indicates high expression, green indicates low expression. (**d**) Volcano plot of common and differentially expressed proteins identified between iPSC-PC/PC. Magenta dots indicate upregulation, grey dots indicate no change and green dots indicate downregulation. (**e-g**) LC/MS quantitative analysis of protein levels shown as donut plots and violin plots of individual biological replicates (top) and phosphorylation (bottom) of canonical pericyte markers (**e**), cell adhesion proteins (**f**) and tight junction proteins (**g**) in iPSC-PC (red) vs. PC (blue). In e-g, n = 6 independent cultures per group; Significance determined by two-stage Benjamini Yekutieli Krieger step up with multiple hypothesis. In **f** and **g**, 5 representative proteins are shown in violin plots.

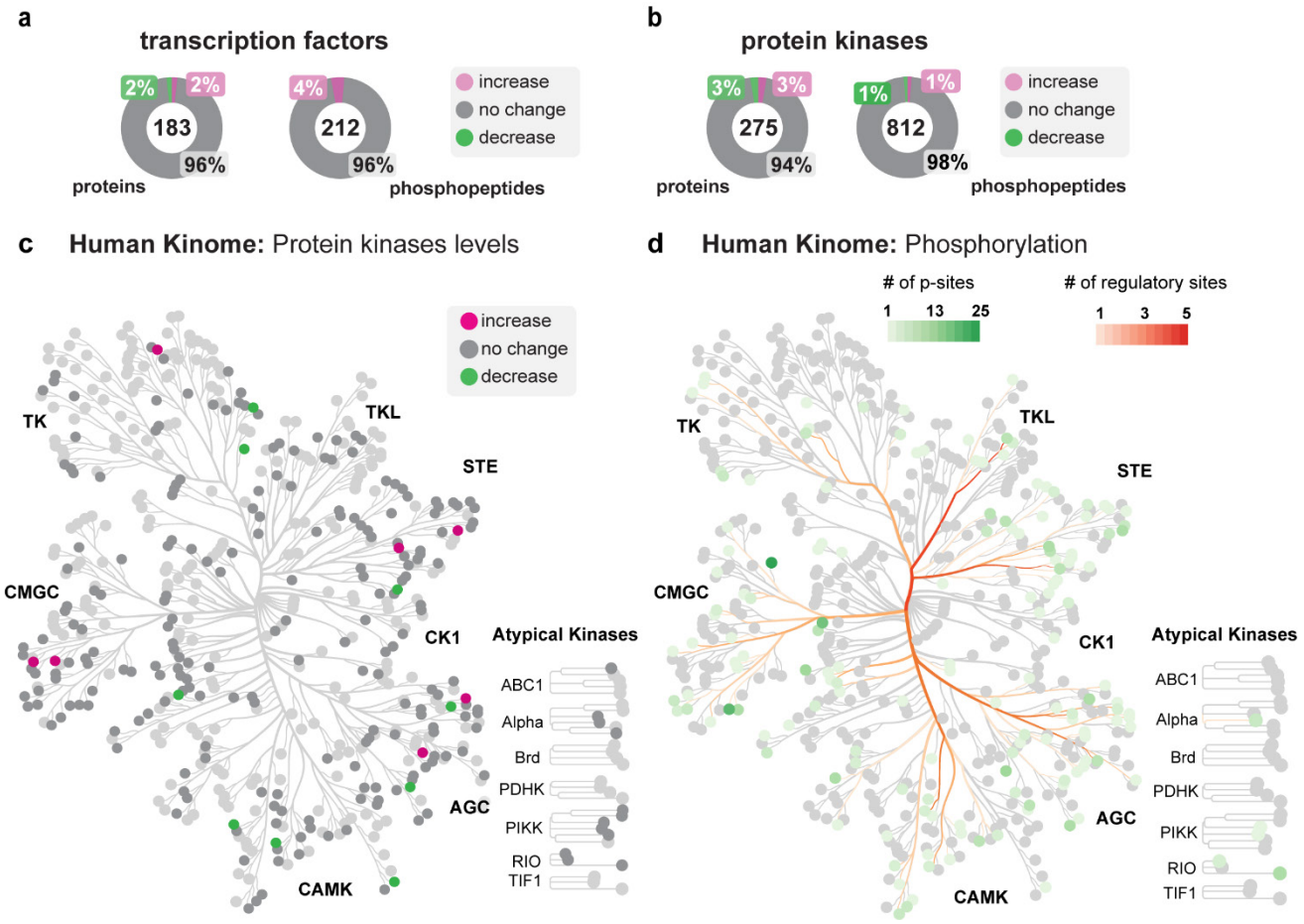

Figure 2. Proteomic analysis of transcription factors and protein kinases in iPSC-PC and PC. (**a**) Quantitative analysis of transcription factor protein levels (left) and phosphorylation (right) in iPSC-PC vs. PC by Liquid Chromatography/Mass Spectrometry (LC/MS). (**b**) LC/MS quantitative analysis of kinase protein levels (left) and phosphorylation (right) in iPSC-PC vs. PC. In **a**, **b**, data shown as donut plots (values inside plots represent total proteins/phosphopeptides; percentage indicates unchanged (grey), downregulated (green) and upregulated (magenta) proteins/phosphopeptides). (**c**) Distribution of protein kinases identified and quantitated in iPSC-PC vs. PC within the human Kinome. Proteins with no changes (gray) and changes (magenta or green) in total protein levels are shown. Light gray: not detected. (**d**) Distribution of unchanged protein kinase phosphorylation sites in iPSC-PC and PC. Green nodes: number of phosphorylation sites identified per protein kinase. Red branches: number of known regulatory sites per individual protein kinase node at the termination of the branch. Light gray: not detected. In **a-d**, n = 6 independent cultures per group; Significance determined by two-stage Benjamini Yekutieli Krieger step up with multiple hypothesis indicated. In **c** and **d**: TK: Tyrosine kinase group; TKL: Tyrosine kinase-like group; STE: Sterile (homologs of yeast Ste7) group; CK1: Casein Kinase 1 group; AGC, Protein kinase A, Protein kinase B, Protein kinase C group; CAMK: Calmodulin calcium kinase group; CMGC: [cyclin-dependent kinases (CDKs), mitogen-activated protein kinases (MAPKs), glycogen synthesis kinases (GSKs), and CDK-like kinases] group.

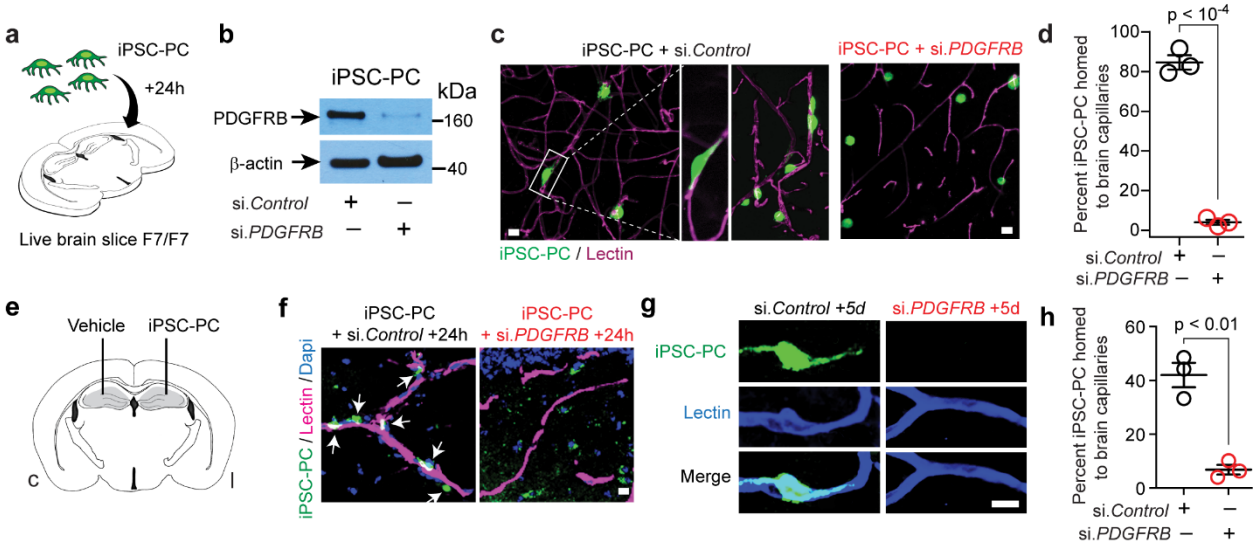

Figure 3. iPSC-PC home to brain capillaries of pericyte-deficient mice to form hybrid human-mouse brain capillaries. (**a**) Schematic showing the *ex vivo* experimental model. GFP-expressing iPSC-PC were added on top of live brain slices from pericyte-deficient *Pdgfrb*$^{F7/F7}$ (F7/F7) mice and were incubated with the tissue for 24 h. (**b**) Immunoblotting for PDGFRβ in iPSC-PC transduced with either control siRNA (si.*Control*) or human *PDGFRB* siRNA (si.*PDGFRB*). (**c-d**). Integration of iPSC-PC-GFP (green) transduced with si.*Control* or si.*PDGFRB* with mouse brain capillaries (Magenta) 24 h after addition to slices (**c**), and quantification of homed iPSC-PC to mouse brain capillaries from 3 independent experiments per treatment (**d**). Scale bar: 50 µm. (**e**) Schematic showing the *in vivo* experimental model. Vehicle (aCSF) or 10^5 GFP-expressing iPSC-PC were stereotaxically injected into the left (**C**, contralateral) and right (**I**, ipsilateral) hippocampus, respectively. (**f-h**) Homing to and integration of iPSC-PC-GFP transduced (green) with either si.*Control* or si.*PDGFRB* with mouse brain capillaries (lectin labeling, magenta; **f**, or blue; **g**) 24 h after transplantation into the hippocampus at a lower (**f**, arrows) and a higher (**g**) magnification, and quantification of homed iPSC-PC to mouse brain capillaries *in vivo* from 3 independent experiments per treatment 5 days after grafting (**h**). Scale bars: 10 µm. Data in **d**, **h** are mean ± SEM; significance by unpaired Student's t test.

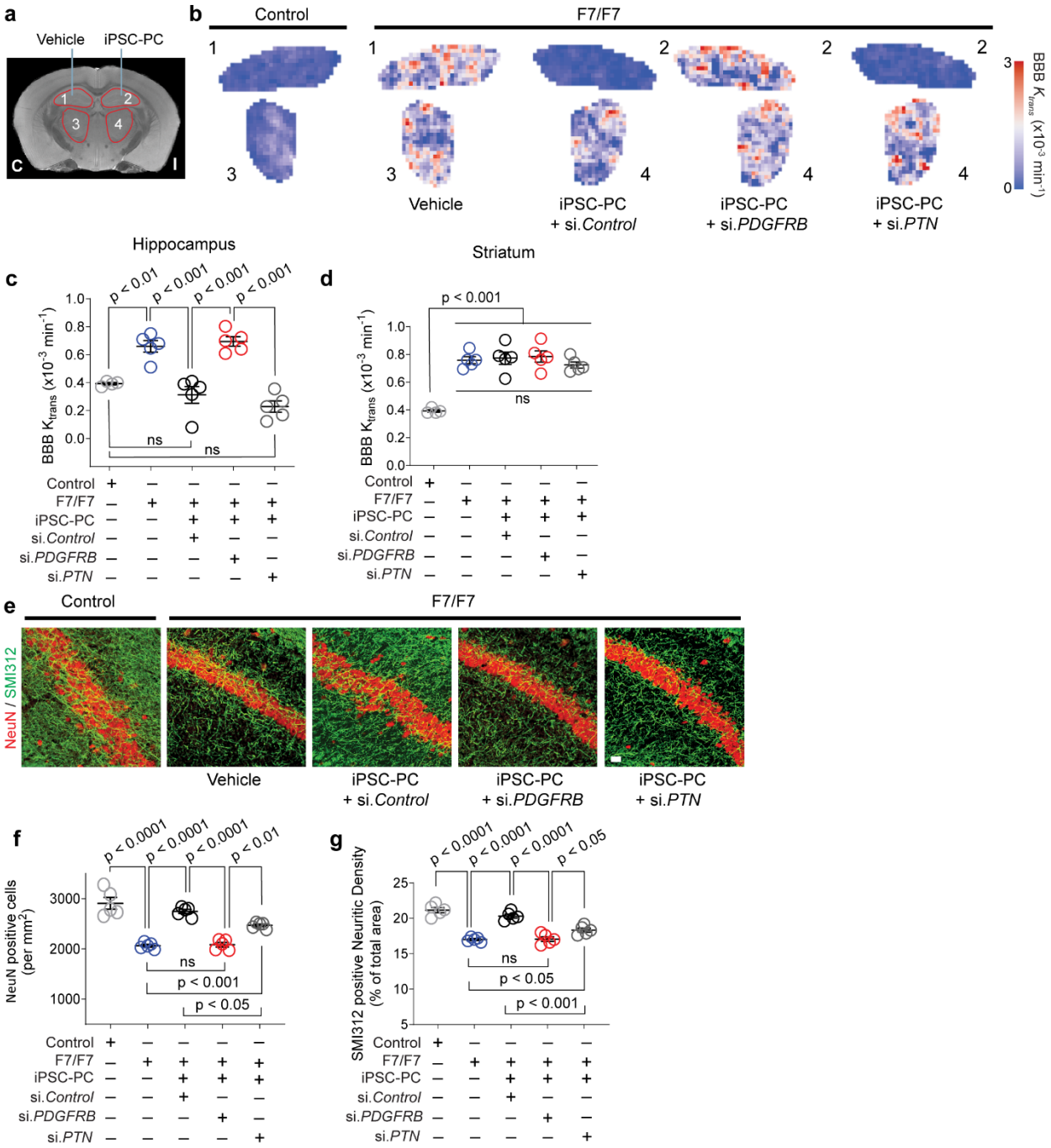

Figure 4. *In vivo* integration of iPSC-PC reduces BBB leakage and improves neuronal retention in the hippocampus of pericyte-deficient mice. (**a**) Schematic showing the *in vivo* experimental model on a T1 map. Vehicle (aCSF) or 10^5 GFP-expressing iPSC-PC were stereotaxically injected into the left (**C**, contralateral) and right (**I**, ipsilateral) hippocampus of 6-8-month old F7/F7 mice, respectively. Hippocampal (**1,2**) and striatal (**3,4**) regions of interest are indicated. (**b-d**) Representative DCE-MRI BBB K_{trans} maps in the hippocampi and striata in control mice (control) and F7/F7 mice treated with vehicle and 5 days after transplantation of iPSC-PC transduced with *si.Control*, *si.PDGFRB* or si.*PTN* (**b**) and quantification of BBB K_{trans} values in the hippocampus (**c**) an striatum (**d**). (**e-g**) Representative confocal microscopy images, scale bar =

50 µm (**e**) and quantification (**f, g**) of NeuN+ neurons (red; **f**) and SMI312+ neurofilaments (green; **g**) in the CA1 hippocampus in control mice and F7/F7 mice treated with vehicle and 5 days after transplantation of iPSC-PC transduced with *si.Control*, *si.PDGFRB* or si.*PTN.* Data in **c**, **d**, **f**, **g** are mean ± SEM; n= 4 control mice in **c**,**d**, and n=5 mice for all other conditions in **c**, **d**, **f**, and **g**. Significance by one-way ANOVA followed by Tukey's posthoc test.

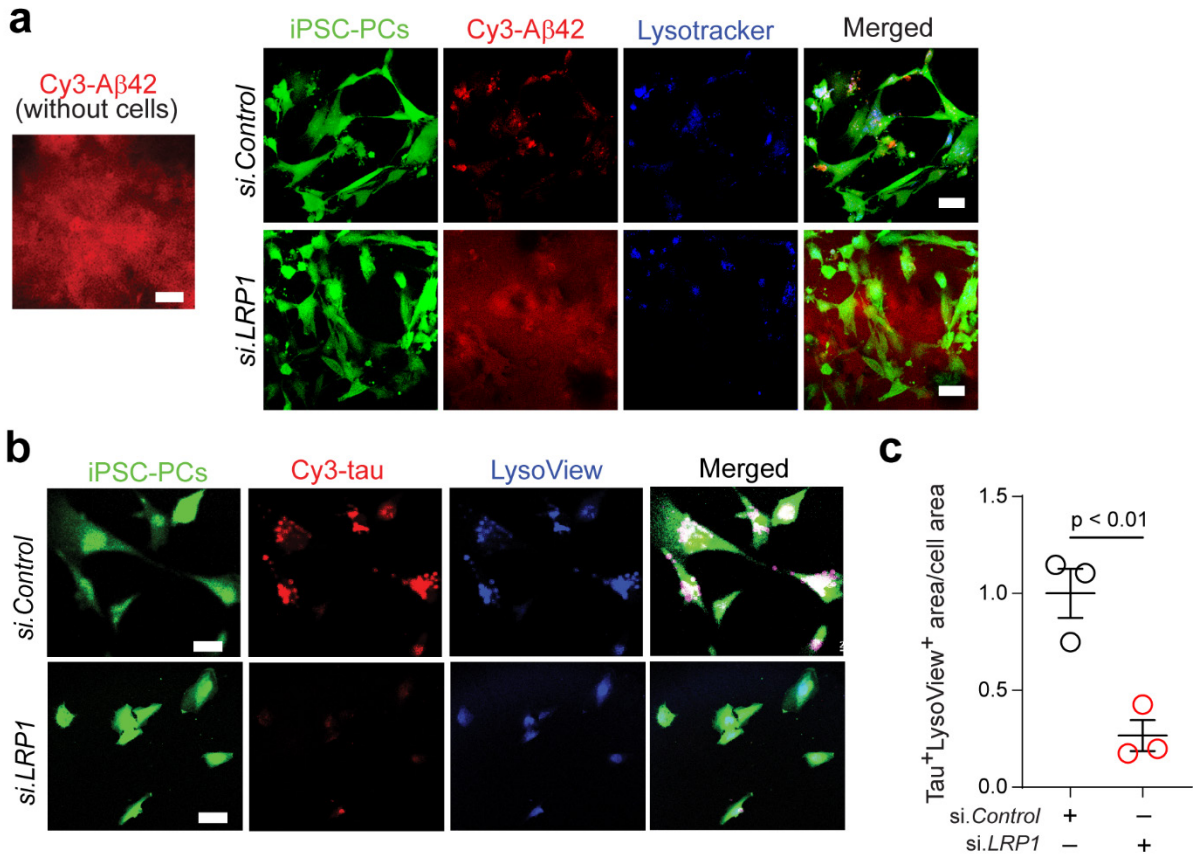

Fig 5. Aβ and tau clearance by iPSC-PC. (**a**) Representative confocal images of multi-spot glass slides coated with Cy3-labeled Aβ42 (red) without cells (far left) and with iPSC-PC (green) after siRNA silencing of *LRP1* (si.*LRP1*) or control siRNA (si.*Control*). Lysosomes are labeled with lysotracker blue (blue). (**b,c**) Representative images of human recombinant Cy3-tau (red) and LysoView 405-positive lysosomes (blue) in iPSC-PC (green) 48h after siRNA silencing of *Lrp1* (si.*LRP1*) or control siRNA (si.*Control*) (**b**), and quantification of lysosomal tau colocalization (**c**). In **c**, data presented as fraction of tau$^+$LysoView$^+$ area relative to total cell area, with all data points normalized to the control mean. Data is mean ± SEM, with n = 3 cultures per condition. Significance by two-tailed t-test. In **a**, **b**, scale bar = 25 µm.